THE JOURNAL OF PHYSICAL CHEMISTRY C

Article

pubs.acs.org/JPCC

Interface Tuning of Current-Induced Cooling in Molecular Circuits

Giuseppe Foti* and Héctor Vázquez*

Institute of Physics, Academy of Sciences of the Czech Republic, Cukrovarnicka 10, Prague, Czech Republic

Supporting Information

ABSTRACT: We study the effect of the atomistic structure of metal−molecule contacts on the current-induced damping and excitation of vibrations in molecular circuits by means of *first-principles* calculations. We consider a carbene-based molecule bound to Au electrodes via three different tip terminations: a tetramer, a pyramid, and a chainlike structure. The change in the width and position of molecular levels associated with each of these metal−molecule structures under an applied voltage controls the heating and cooling processes. In blunt tips, where the electronic coupling between molecular and Au bulk states is strong, the cooling efficiency decreases as a function of bias which results in the heating of the most active vibrational modes. On the other hand, in chainlike structures where the coupling is weak, the cooling rate has a nonmonotonic behavior as a function of the applied bias and increases sharply beyond a certain voltage. This results in a current-induced cooling at high bias. These findings open the way to the efficient removal of excess heat from the junction through control of the metal−molecule contact structures.

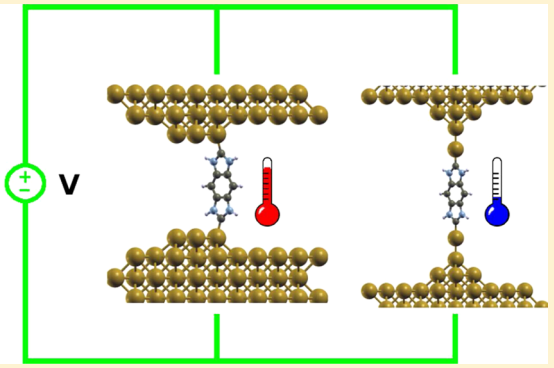

INTRODUCTION

The field of molecular electronics has reached a mature stage, and great progress has been made in the understanding of the different mechanisms controlling charge transport in single molecule junctions.[1−4] However, one of the main obstacles hampering the development of molecular scale circuits is the stability of nanojunctions under an applied bias. Because of the reduced dimensionality of the system, the junction has to sustain very high current densities which can generate extremely high temperatures. This can promote conformational changes of the junction[5−10] or induce its breakdown.[11−14] Thus, it is of paramount importance to go beyond the elastic charge transport picture and develop a detailed understanding of the processes controlling how heat is generated and dissipated in molecular junctions. Current-induced cooling via specific vibrational modes was recently studied using density functional tight-binding methods.[15] In this work we show how the atomistic structure of the metal−molecule interface plays a fundamental role in determining the heating and cooling dynamics (HCD) of molecular junctions under an external bias and how it can be used to efficiently dissipate heat at the junction.

Electrons tunneling through a molecular junction can exchange energy with the vibrations of the molecule. They can release energy into the vibrational modes, which increases the temperature of the molecule. These interactions are responsible for the Joule heating mechanism[16−20] of the junction. Electrons can also absorb energy from the vibrational modes of the molecule and cool it down. These current-induced and electron−hole[21,22] damping of molecular vibrations represent, among other mechanisms,[23] an important cooling channel for the system and contribute to the stabilization of the junction in a out-of-equilibrium situation. Figure 1 summarizes the current-induced emission and absorption processes of localized vibrations in a molecular junction under an applied bias. In this schematic junction, conductance is dominated by the lowest unoccupied molecular orbital (LUMO). Solid lines show the left- and right-projected molecular density of states (DOS). Tunneling electrons

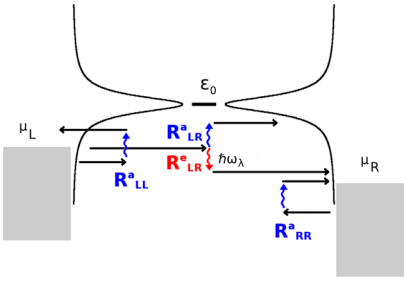

Figure 1. Schematics of the current-induced inelastic processes in a molecular junction under an applied bias. ϵ_0 denotes a molecular resonance while μ_L and μ_R are the chemical potentials of the left and right electrodes, respectively. Black curves are the left- and right-projected DOS while black arrows specify the direction of propagation of tunneling electrons. Blue arrows indicate intraelectrode (R^a_{LL}, R^a_{RR}) and interelectrode (R^a_{LR}) absorption of vibrational quanta while the red arrow represents emission (R^e_{LR}).

Received: November 28, 2016
Revised: December 21, 2016
Published: December 22, 2016

DOI: 10.1021/acs.jpcc.6b11955
J. Phys. Chem. C 2017, 121, 1082−1088

(arrows) can interact with localized molecular vibrations. The red arrow indicates the emission of molecular vibrations (R^{e}_{LR}), whereby the electron releases some energy which is absorbed by the vibrational degrees of freedom, contributing to the local heating of the junction. Blue arrows represent the processes of absorption of vibrations, which cool the junction by transferring energy from the vibrational to the electronic degrees of freedom. Electrons can also absorb energy from localized vibrations and be backscattered into the leads. These intraelectrode processes are represented by the R^{a}_{LL} and R^{a}_{RR} symbols. Absorption processes can also be associated with interelectrode scattering. R^{a}_{LR} in Figure 1 represents the absorption of vibrational energy of a right-moving electron which tunnels into the right electrode at a higher energy. In absorption processes the excess energy of the electrons is released in the electrodes[24] far from the junction. However, emission processes result in vibrations localized at the interface molecule. At equilibrium, the population of molecular vibrations is given by the Bose−Einstein distribution.[25] An applied bias drives the vibronic system in the device region out of equilibrium. However, if the absorption processes dominate over emission, the system is stable and the vibration population reaches a steady state condition.

The physical picture described in Figure 1 depends strongly on the width and position of the molecular resonance controlling charge transport.[24,26−29] In general, the closer the LUMO is to the Fermi level (FL), the stronger absorption processes are. On the other hand, a high DOS in the proximity of the bias window, associated with a strong electronic coupling of molecular and metal states, enhances the emission processes. Thus, the interplay of width and position of the molecular resonance defines the onset and intensity of the energy exchange between electronic and vibrational degrees of freedom.

Here we illustrate this interplay for a series of molecular junctions formed by N-heterocyclic carbenes (NHCs) where charge transport is dominated by the tail of the LUMO resonance. NHCs have attracted much attention for their interesting properties.[30] NHCs are highly reactive σ donors, and on gold, they have shown to be chemically stable at high temperatures.[31] The binding of NHCs to Au is particularly interesting in the field of molecular electronics since covalent Au−C metal−molecule bonds were shown to result in highly conducting junctions.[32−35] Recently we studied the transport properties of this NHC-based molecule on Au(100).[36] We found clear trends between the LUMO position and the atomistic details of the tip termination. Longer tips with a low coordination number of the Au contact atom induce a more pronounced downshift of the LUMO than for blunt ones. This structure-dependent downshift of molecular levels effectively acts as a gating potential and results in an 8-fold change of conductance at the FL. Here we focus on the effect of the atomistic structure of the metal−molecule interface on current-induced emission and damping of molecular vibrations. We consider three specific junction structures on Au(100), namely, a tetramer, a pyramid, and a chainlike termination. This last geometry models the final stages in pulling experiments with strong metal−molecule bonds where, before rupture, Au atoms are detached from the surface. In these stretched configurations, mechanical or current-induced perturbations can induce the breaking of the junction.

For these NHC-based junctions, we calculate the rates of emission and absorption of molecular vibrations as a function of the applied bias. The ratio of the absorption to emission rates controls the HCD of the junction due to the interaction of the electronic system with the localized vibrations of the molecule. We find that for the chainlike junction the presence of a sharp LUMO resonance close to the FL enhances the current-induced absorption of vibrations compared to blunt tips. These findings highlight the critical role of electrode termination in the current-induced HCD of carbene-based junctions and point to the remarkable cooling dynamics of highly stretched molecular junctions.

METHOD

The emission and absorption of molecular vibrations due to the interaction with the electronic system can be described in the framework of the nonequilibrium Green's function (NEGF) theory.[25,27,37] In the low temperature limit the vibron emission rate $R^{e,\lambda}_{LR}$ (where energy is transferred from the electrons to the vibrational mode λ) is expressed as

$$R^{e,\lambda}_{LR} = \int_{\mu_R+\hbar\Omega}^{\mu_L} \Lambda^{\lambda}_{L,R}(\epsilon, \epsilon - \hbar\Omega)\, d\epsilon \tag{1}$$

while the vibron absorption processes are given by the following terms:

$$\begin{aligned} R^{a,\lambda} = &\int_{\mu_R-\hbar\Omega}^{\mu_L} \Lambda^{\lambda}_{L,R}(\epsilon, \epsilon + \hbar\Omega)\, d\epsilon \\ &+ \int_{\mu_L-\hbar\Omega}^{\mu_L} \Lambda^{\lambda}_{L,L}(\epsilon, \epsilon + \hbar\Omega)\, d\epsilon \\ &+ \int_{\mu_R-\hbar\Omega}^{\mu_R} \Lambda^{\lambda}_{R,R}(\epsilon, \epsilon + \hbar\Omega)\, d\epsilon = R^{a,\lambda}_{LR} + R^{a,\lambda}_{LL} + R^{a,\lambda}_{RR} \end{aligned} \tag{2}$$

We calculate the terms $\Lambda^{\lambda}_{\alpha,\beta}(\epsilon,\epsilon')$ as

$$\Lambda^{\lambda}_{\alpha,\beta}(\epsilon, \epsilon') = \frac{1}{2\pi\hbar}\mathrm{Tr}[\mathbf{M}^{\lambda}(\Gamma)\langle \mathbf{A}_{\alpha}(\epsilon, k)\rangle_k \mathbf{M}^{\lambda}(\Gamma)\langle \mathbf{A}_{\beta}(\epsilon', k)\rangle_k] \tag{3}$$

where α, β = L, R. The matrices $\mathbf{A}_{\alpha,\beta}(\epsilon,k)$ are the left and right spectral functions which are related to the density of states projected onto the left and right side of the junction, respectively.[38] In the most general case these functions depend on both energy ϵ and electron momentum k. The spectral functions also depend on the applied bias through the nonequilibrium potential across the junction. To alleviate the notation, we omit this dependence in eq 3. Here we approximate the $\Lambda^{\lambda}_{\alpha,\beta}(\epsilon,\epsilon')$ functions by making an average over electron momentum of the spectral functions in order to properly take into account the electronic structure. This approach is essential to avoid unphysical, sharp discontinuities of the rates as a function of bias. For the calculation of the electron−phonon coupling matrix $\mathbf{M}(q,k)$,[39] which depends on both the electron and phonon momentum (q), we use the $\mathbf{M}(\Gamma)$ approximation[40] which consists on calculating $\mathbf{M}$ in the Γ point of the Brillouin zone for both electrons and phonons. For systems with localized vibrations such as single molecule junctions or dilute molecular monolayers the $q = 0$ approximation has proven to be reliable due to the weak dispersion of vibrational modes in the plane perpendicular to transport. Also, the k dependence of the $\mathbf{M}$ matrix can be avoided through and adequate choice of representation of the Hamiltonian and overlap matrices.[40]

The HCD of the molecule as a function of the applied bias can be captured by solving a steady-state equation for the

DOI: 10.1021/acs.jpcc.6b11955
J. Phys. Chem. C 2017, 121, 1082−1088

vibron populations[41] which, in the undamped limit (no dissipation of energy into bulk phonons), is inversely proportional to the ratio between absorption and emission rates:

$$R^{\lambda}(V) = \frac{R^{a,\lambda}(V)}{R^{e,\lambda}_{LR}(V)} \quad (4)$$

A ratio higher than one indicates a net energy transfer from the vibrational to the electronic degrees of freedom, effectively cooling down the junction. On the other hand, if the current-induced emission dominates over the electronic damping, the ratio $R^{\lambda}(V)$ is lower than one and, at that bias, the vibronic population grows as a function of time, resulting in a strong increase of the effective temperature of the molecule. These vibrational instabilities[27,42,43] eventually lead to the breaking of the junction.

Figure 2a shows the NHC-based molecule considered in this study. It is has two imidazole groups connected by a central benzene ring. Figure 2b–d shows the three structures considered: with the Au tip atoms forming a tetramer (b), a pyramidal structure (c), or an elongated, chainlike structure with a Au atom above a pyramid (d). These structures are hereafter referred to as T, P, and C, respectively. This latter binding motif is motivated by our recent pulling simulations of carbenes over Au(111) surface where, due to the strong Au–C bond, the contact Au atom can be extracted from the surface forming a short monatomic Au chain before the junction rupture. This behavior has been observed in a large variety of thiol-functionalized molecules anchored to Au or Pt electrodes.[44−49]

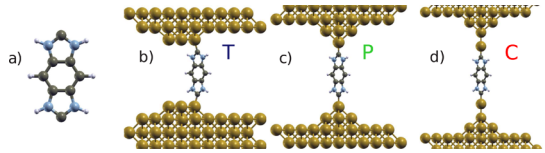

Figure 2. Schematics of (a) the NH-based carbene and (b–d) the three structures studied. Gray atoms = carbons, white atoms = hydrogens, and blue atoms = nitrogens. The metal–molecule contact is described by (b) tetramers, (c) pyramids, and (d) chainlike structures.

In the calculation of the electronic and charge transport properties[50,51] we use a single-ζ plus polarization basis for gold and a double-ζ plus polarization basis for sulfur, hydrogen, and carbon atoms. Exchange correlation is described with the generalized gradient approximation (GGA).[52] The positions of the molecule, tip atoms, and the surface gold layers were relaxed until residual forces fell below 0.02 eV/Å using a $k = 5 \times 5 \times 1$ Monkhorst–Pack grid for the calculation of the electronic structure. Eigenchannels are calculated following the method of Paulsson and Brandbyge.[53] In order to compute the emission and absorption rates in a out-of-equilibrium situation, it is mandatory to properly describe the bias dependence of the electronic structure of the full system. We thus calculated the electronic structure of the molecular junction self-consistently for different values of an applied bias up to 1.2 V in steps of 0.2 V.

SPECTRAL FUNCTIONS AND THEIR BIAS DEPENDENCE

We begin by analyzing the equilibrium (zero bias) electronic structure of the junctions. Figure 3 shows the projection of the left and right spectral function matrices onto the molecular subspace for the three structures considered at zero bias. This quantity shows how the position and broadening of the main (LUMO-derived) resonance changes as a function of the tip structure. For the T geometry the resonance is located at relatively high energies (1.2 eV) which results in a low density of states at the FL. In the case of the P geometry, the resonance is rigidly shifted down in energy to 0.6 eV, having approximately the same broadening. As a consequence, the density of states at the FL is higher compared to the T junction. For the chainlike structure the resonance is at even lower energies (0.45 eV), but the small electronic coupling arising from the reduced hybridization of the Au contact atom results into a low DOS at the FL.[36] These differences give rise to different HDC for the three structures in the presence of an external bias.

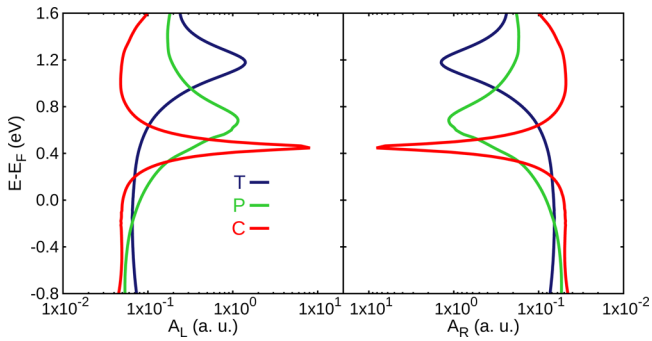

Figure 3. Zero bias left and right spectral functions projected onto the molecular orbitals for the three junction structures considered.

In order to investigate the HCD, it is necessary to know how the position of molecular resonances changes under an applied bias since the processes shown in Figure 1 strongly depend on the DOS near the FL. According to the selection rules,[48,54−59] the most intense inelastic scattering processes for this kind of junction involve channels with different (π and σ) symmetries. Figure 4 shows the left and right spectral functions for the C geometry decomposed into σ and π channels at 0 and 1.2 V. In

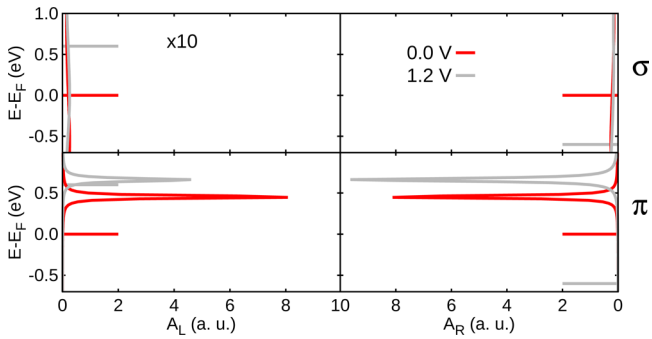

Figure 4. Left and right spectral functions for the C geometry decomposed into σ (upper panels) and π (lower panels) channels at 0 and 1.2 V (red and gray lines, respectively). Notice that the scale for the σ channel is expanded by a factor 10. Horizontal lines define the left and right chemical potentials.

DOI: 10.1021/acs.jpcc.6b11955
J. Phys. Chem. C 2017, 121, 1082−1088

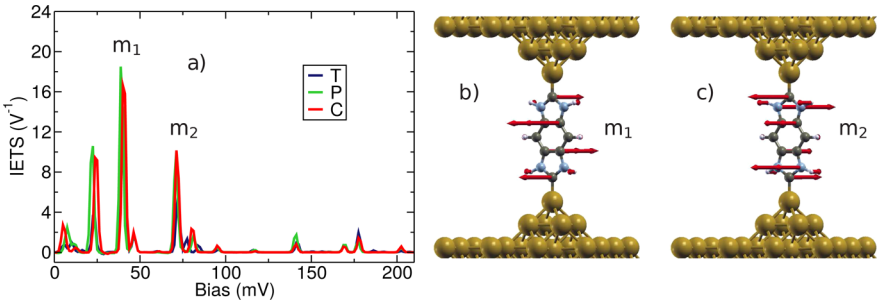

Figure 5. (a) IETS for the three structures considered. The labels m_1 and m_2 indicate the most active modes of the junction above the energy of bulk phonons of Au. Panels (b) and (c) show modes m_1 and m_2, respectively.

this energy range, the σ channel is very smooth while the π channel shows a sharp peak at the molecular resonance which moves toward higher energies when a finite bias is applied. A more detailed study of the pinning of the σ- and π-projected spectral functions for the three structures in the whole bias interval is reported in the Supporting Information.

IDENTIFICATION OF ACTIVE VIBRATIONAL MODES

The sets of eqs 1 and 2 are computationally very expensive to calculate due to the energy integration and the necessary k-point averaging of the spectral functions over the first Brillouin zone. Thus, it becomes mandatory to restrict the analysis to a small number of vibrational modes for which the heating mechanism is more critical. We characterize the vibrational modes and inelastic spectrum of the three structures under study and focus on the most active ones with the highest heating rate. From the calculated inelastic electron tunneling spectra (IETS)[39] (Figure 5a), we can identify the most relevant vibrational modes, which are at 25, 40, and 71 meV. In the bulk, Au phonons have a cutoff energy of approximately 25 meV.[60] Molecular vibrations with an energy equal to or lower than this threshold can dissipate the excess heat into these modes.[61] Above this cutoff the damping of vibrons is less effective due to energy mismatch. We will therefore focus on the two modes at 40 and 71 meV for which the energy exchange with the electronic bath is more critical for the thermal stability of the junction. For all structures the two peaks at 40 and 71 meV (indicated by the labels m_1 and m_2 in Figure 5a) are given by interchannel processes and are associated with the out-of-plane modes shown in Figure 5b,c. In the Supporting Information we resolve the contributions to the IETS signal arising from the different symmetries.

We also restrict our analysis to the bias regime where phase space for excitation of high-energy modes is much lower than for absorption (up to 1.2 V). At the vibrational threshold $[eV_b = e(\mu_L - \mu_R) = \hbar\omega_\lambda]$ and at zero temperature, only electrons with $\epsilon = \mu_L$ can dissipate energy into mode λ and tunnel inelastically into the right electrode. Electrons with an incident energy lower than μ_L cannot emit the quantum of energy $\hbar\omega_\lambda$ since on the right electrode there are no empty states below $\mu_L - \hbar\omega_\lambda$. On the other hand, the energy window for absorption processes is much larger, spanning from $\mu_R - \hbar\omega_\lambda$ to μ_L. This makes the cooling of high-energy modes at low bias particularly effective. We neglect the dissipation due to anharmonic coupling between molecular vibrations as this has been shown to be negligible in molecular junctions at room temperature.[62]

EMISSION AND ABSORPTION RATES

As mentioned before, in the presence of an external bias, tunneling electrons drive the vibrational system out of equilibrium, heating the junction. If the total absorption rate is higher than emission, a steady-state condition for vibron populations is established, in which the population of molecular vibrations is constant in time and the system is stable. Figure 6

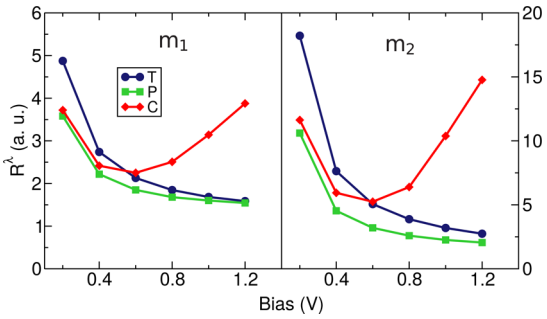

Figure 6. Calculated cooling rates of modes m_1 and m_2 for the three structures considered as a function of applied voltage. The higher the rate, the more efficient the cooling of vibrational modes by the tunneling electrons.

shows the ratio of absorption to emission (eq 4) for modes m_1 and m_2 as a function of applied bias for the three structures considered. In all cases the ratio eq 4 is always higher than one in the whole bias range considered which means that no current-induced vibrational instabilities take place and the systems are all stable in the nonequilibrium condition. The trend of R^λ as a function of bias is the same for both modes m_1 and m_2. R^λ shows two distinct tendencies as a function of bias depending on the metal−molecule interface geometry. For blunt tips (T and P structures) the net rate decreases monotonically as bias is increased. This means that the higher the bias, the less effective the electronic cooling of the vibrational modes is. This results in an increase of the effective temperature of the vibrational mode as a function of bias. For the elongated C structure, on the other hand, the net rate has a more complex behavior. At low biases, the ratio between absorption and emission rates first decreases but then rises above 0.6 V. This increase results in an effective cooling of the most active vibrational modes and in a reduction of their effective temperature. We can understand this trend by examining the contributions of the different emission and absorption processes (eqs 1 and 2) to the rate R^λ. These are shown in Figure 7 for mode m_1, and a similar analysis is done in the Supporting Information for mode m_2. For both T and P structures, the width and position of the LUMO resonance are

DOI: 10.1021/acs.jpcc.6b11955
J. Phys. Chem. C 2017, 121, 1082−1088

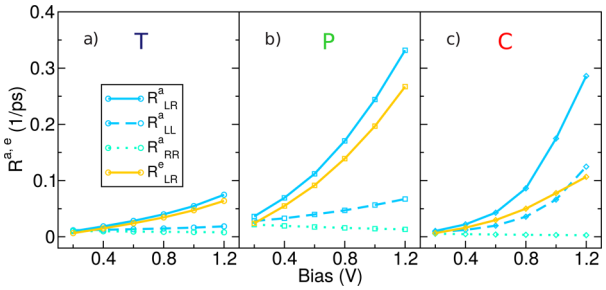

Figure 7. Emission and absorption rates as a function of bias for mode m_1 for the three structures.

such that at any given voltage interelectrode emission and absorption rates R^e_{LR} and R^a_{LR} are not too different from each other, and their ratio is approximately constant as a function of bias. The intraelectrode absorption process on the left contact (R^a_{LL}), on the other hand, shows a modest increase while on the right electrode the R^a_{RR} rate decreases. As a result, the ratio R^λ in eq 4, which involves all absorption processes, decreases as a function of bias, and the effective temperature of the two modes increases. Among the T and P structures, the lower LUMO position in the P case gives rise to higher contributions for this structure.

The C geometry, however, has a lower lying LUMO than the two other junctions but an even narrower peak due to the small electronic coupling of this elongated structure. Thus, the ratio of the resonance position to its width is highest for the chainlike geometry. This means that the onset of processes involving the peak of this resonance will be sudden. This is reflected in the faster increase of R^a_{LR} and R^a_{LL} at high voltages compared to the T and P structures (Figure 7). When the applied bias is such that the chemical potential approaches the LUMO energy $[eV_b/2 = \mu_L \simeq (\epsilon_0 - \hbar\omega_\lambda)]$, the absorption processes involving the molecular resonance R^a_{LR} and R^a_{LL} are enhanced substantially. The other (emission and absorption) processes R^e_{LR} and R^a_{RR} are not so efficient due to the low DOS at the energy of the outgoing electron. This is seen in the clear increase of R^a_{LR} and R^a_{LL} at high voltages, while the increase in the emission term R^e_{LR} is much lower. The net balance of these terms results in the nonmonotonic behavior of the cooling rate R^λ of the C junction in the high bias region (Figure 6). Notice that the same physical mechanism applies to the T and P structures, but the lower slope of the DOS around the bias window makes these effects smoother. For these structures, the DOS at $\epsilon + \hbar\omega_\lambda$ and $\epsilon - \hbar\omega_\lambda$ are not so different, and thus their impact on the ratio in eq 4 is lower, resulting in a monotonic reduction of R^λ as a function of bias.

CONCLUSIONS

We studied the current-induced emission and absorption of molecular vibrations in a series of carbene-based molecular junctions. In these systems, the width and position of the frontier molecular orbital controlling transport can be tuned through the atomistic structure of the metal−molecule interface. We considered tetrameric, pyramidal, and chainlike terminations. We found that the changes in the electronic structure associated with these different contacts determine the current-induced heating and cooling of the junction through the emission and damping of localized molecular vibrations. Broad molecular resonances, associated with strong metal−molecule electronic coupling, result in small differences of the molecular DOS in the range of inelastic processes. As a consequence, the cooling ratio (of absorption to emission rates) decreases monotonically as a function of the applied voltage. Elongated tip structures with low coordination Au atoms, however, give rise to sharp molecular resonances. Here the rates of emission and absorption processes are very different depending on whether they are resonant with the molecular states or not. For LUMO-derived conductance, this results in a nonmonotonic behavior of the net cooling ratio which increases sharply beyond a given voltage, effectively cooling the junction at high voltages.

Our results highlight the important role played by the atomistic details of the metal−molecule contacts not only on the electronic and elastic transport properties of carbene-based junctions but also on the energy exchange between electronic and vibrational degrees of freedom under an applied bias. They reveal trends between the tip shape and the heating and cooling ability and, in particular, state the somewhat counterintuitive idea that elongated chainlike structures provide the highest current-induced cooling of molecular vibrations at high voltages. These stretched junctions can be formed in the final stages before rupture of pulling experiments, and their stability is therefore critical. Since electronic damping of molecular vibrations is an important cooling channel, it effectively stabilizes the junction. We believe our results to be relevant for a broader range of molecular junctions having strong metal−molecule bonds and sharp resonances close to the FL.

ASSOCIATED CONTENT

Supporting Information

The Supporting Information is available free of charge on the ACS Publications website at DOI: 10.1021/acs.jpcc.6b11955.

Bias dependence of the σ- and π-projected spectral functions; characterization of the vibrational modes; emission and absorption rates for mode m_2 (PDF)

AUTHOR INFORMATION

Corresponding Authors

*E-mail: foti@fzu.cz (G.F.).
*E-mail: vazquez@fzu.cz (H.V.).

ORCID

Giuseppe Foti: 0000-0001-5769-2253

Notes

The authors declare no competing financial interest.

ACKNOWLEDGMENTS

We gratefully acknowledge financial support from the Czech Science Foundation (GAČR) under project 15-19672S, the Purkyně Fellowship program of the Academy of Sciences of the Czech Republic, and the Horizon 2020 research and innovation program under the Marie Skłodowska-Curie grant agreement no. 709114. Computational resources were provided by CESNET LM2015042 and CERIT Scientific Cloud LM2015085, under the program "Projects of Large Research, Development, and Innovations Infrastructure".

REFERENCES

(1) Cuevas, J. C.; Scheer, E. *Molecular Electronics: An Introduction to Theory and Experiment*; World Scientific Publishing Co. Pte. Ltd.: 2010.

(2) Tao, N. J. Electron Transport in Molecular Junctions. *Nat. Nanotechnol.* **2006**, *1*, 173−181.

DOI: 10.1021/acs.jpcc.6b11955
J. Phys. Chem. C 2017, 121, 1082−1088

(3) Aradhya, S. V.; Venkataraman, L. Single-Molecule Junctions Beyond Electronic Transport. *Nat. Nanotechnol.* **2013**, *8*, 399−410.
(4) Capozzi, B.; Xia, J.; Adak, O.; Dell, E. J.; Liu, Z.-F.; Taylor, J. C.; Neaton, J. B.; Campos, L. M.; Venkataraman, L. Single-Molecule Diodes with High Rectification Ratios Through Environmental Control. *Nat. Nanotechnol.* **2015**, *10*, 522−527.
(5) Komeda, T.; Kim, Y.; Kawai, M.; Persson, B. N. J.; Ueba, H. Lateral Hopping of Molecules Induced by Excitation of Internal Vibration Mode. *Science* **2002**, *295*, 2055−2058.
(6) Qiu, X. H.; Nazin, G. V.; Ho, W. Mechanisms of Reversible Conformational Transitions in a Single Molecule. *Phys. Rev. Lett.* **2004**, *93*, 196806.
(7) Liljeroth, P.; Repp, J.; Meyer, G. Current-Induced Hydrogen Tautomerization and Conductance Switching of Naphthalocyanine Molecules. *Science* **2007**, *317*, 1203−1206.
(8) Jia, X.; Hofmann, M.; Meunier, V.; Sumpter, B. G.; Campos-Delgado, J.; Romo-Herrera, J. M.; Son, H.; Hsieh, Y.-P.; Reina, A.; et al. K. Controlled Formation of Sharp Zigzag and Armchair Edges in Graphitic Nanoribbons. *Science* **2009**, *323*, 1701−1705.
(9) Lau, C. S.; Mol, J. A.; Warner, J. H.; Briggs, G. A. D. Nanoscale Control of Graphene Electrodes. *Phys. Chem. Chem. Phys.* **2014**, *16*, 20398−20401.
(10) Xiang, L.; Tao, N. J. Organic Chemistry: Reactions Triggered Electrically. *Nature* **2016**, *531*, 38−39.
(11) Huang, Z.; Xu, B.; Chen, Y.; Di Ventra, M.; Tao, N. J. Measurement of Current-Induced Local Heating in a Single Molecule Junction. *Nano Lett.* **2006**, *6*, 1240−1244.
(12) Dundas, D.; McEniry, E. J.; Todorov, T. N. Current-Driven Atomic Waterwheels. *Nat. Nanotechnol.* **2009**, *4*, 99−102.
(13) Santini, C. A.; Vereecken, P. M.; Volodin, A.; Groeseneken, G.; De Gendt, S.; Haesendonck, C. V. A Study of Joule Heating-Induced Breakdown of Carbon Nanotube Interconnects. *Nanotechnology* **2011**, *22*, 395202.
(14) Sabater, C.; Untiedt, C.; van Ruitenbeek, J. M. Evidence for Non-Conservative Current-Induced Forces in the Breaking of Au and Pt Atomic Chains. *Beilstein J. Nanotechnol.* **2015**, *6*, 2338−2344.
(15) Lykkebo, J.; Romano, G.; Gagliardi, A.; Pecchia, A.; Solomon, G. C. Single-Molecule Electronics: Cooling Individual Vibrational Modes by the Tunneling Current. *J. Chem. Phys.* **2016**, *144*, 114310.
(16) Galperin, M.; Ratner, M. A.; Nitzan, A. Molecular Transport Junctions: Vibrational Effects. *J. Phys.: Condens. Matter* **2007**, *19*, 103201.
(17) Huang, Z.; Chen, F.; D'agosta, R.; Bennett, P. A.; Di Ventra, M.; Tao, N. J. Local Ionic and Electron Heating in Single-Molecule Junctions. *Nat. Nanotechnol.* **2007**, *2*, 698−703.
(18) Pecchia, A.; Romano, G.; Di Carlo, A.; Gagliardi, A.; Frauenheim, T. Joule Heating in Molecular Tunnel Junctions: Application to C60. *J. Comput. Electron.* **2008**, *7*, 384−389.
(19) Engelund, M.; Fürst, J. A.; Jauho, A. P.; Brandbyge, M. Localized Edge Vibrations and Edge Reconstruction by Joule Heating in Graphene Nanostructures. *Phys. Rev. Lett.* **2010**, *104*, 036807.
(20) Ward, D. R.; Corley, D. A.; Tour, J. M.; Natelson, D. Vibrational and Electronic Heating in Nanoscale Junctions. *Nat. Nanotechnol.* **2011**, *6*, 33−38.
(21) Persson, B.; Persson, M. Damping of Vibrations in Molecules Adsorbed on a Metal Surface. *Surf. Sci.* **1980**, *97*, 609−624.
(22) Head-Gordon, M.; Tully, J. C. Molecular Dynamics with Electronic Frictions. *J. Chem. Phys.* **1995**, *103*, 10137−10145.
(23) Galperin, M.; Saito, K.; Balatsky, A. V.; Nitzan, A. Cooling Mechanisms in Molecular Conduction Junctions. *Phys. Rev. B: Condens. Matter Mater. Phys.* **2009**, *80*, 115427.
(24) Lee, W.; Kim, K.; Jeong, W.; Zotti, L. A.; Pauly, F.; Cuevas, J. C.; Reddy, P. Heat Dissipation in Atomic-Scale Junctions. *Nature* **2013**, *498*, 209−212.
(25) Pecchia, A.; Romano, G.; Di Carlo, A. Theory of Heat Dissipation in Molecular Electronics. *Phys. Rev. B: Condens. Matter Mater. Phys.* **2007**, *75*, 035401.
(26) Romano, G.; Gagliardi, A.; Pecchia, A.; Di Carlo, A. Heating and Cooling Mechanisms in Single-Molecule Junctions. *Phys. Rev. B: Condens. Matter Mater. Phys.* **2010**, *81*, 115438.
(27) Lü, J.-T.; Hedegård, P.; Brandbyge, M. Laserlike Vibrational Instability in Rectifying Molecular Conductors. *Phys. Rev. Lett.* **2011**, *107*, 046801.
(28) Franke, K. J.; Pascual, J. I. Effects of Electron-Vibration Coupling in Transport through Single Molecules. *J. Phys.: Condens. Matter* **2012**, *24*, 394002.
(29) Kaasbjerg, K.; Novotny, T.; Nitzan, A. Charge-Carrier-Induced Frequency Renormalization, Damping, and Heating of Vibrational Modes in Nanoscale Junctions. *Phys. Rev. B: Condens. Matter Mater. Phys.* **2013**, *88*, 201405.
(30) Arduengo, A. J., III; Harlow, R. L.; Kline, M. A Stable Crystalline Carbene. *J. Am. Chem. Soc.* **1991**, *113*, 361−363.
(31) Crudden, C. M.; Horton, J. H.; Ebralidze, I. I.; Zenkina, O. V.; McLean, A. B.; Drevniok, B.; She, H.-B.; Kraatz, Z.; Mosey, N. J.; Seki, T.; et al. Ultra Stable Self-Assembled Monolayers of N-Heterocyclic Carbenes on Gold. *Nat. Chem.* **2014**, *6*, 409−414.
(32) Cheng, Z.-L.; Skouta, R.; Vázquez, H.; Widawsky, J.; Schneebeli, S.; Chen, L. W. S.; Hybertsen, M.; Breslow, R.; Venkataraman, L. In Situ Formation of Highly Conducting Covalent Au-C Contacts for Single-Molecule Junctions. *Nat. Nanotechnol.* **2011**, *6*, 353−357.
(33) Chen, W.; Widawsky, J. R.; Vázquez, H.; Schneebeli, S. T.; Hybertsen, M. S.; Breslow, R.; Venkataraman, L. Highly Conducting π-Conjugated Molecular Junctions Covalently Bonded to Gold Electrodes. *J. Am. Chem. Soc.* **2011**, *133*, 17160−17163.
(34) Widawsky, J. R.; Chen, W.; Vázquez, H.; Kim, T.; Breslow, R.; Hybertsen, M. S.; Venkataraman, L. Length-Dependent Thermopower of Highly Conducting Au-C Bonded Single Molecule Junctions. *Nano Lett.* **2013**, *13*, 2889−2894.
(35) Foti, G.; Vázquez, H.; Sánchez-Portal, D.; Arnau, A.; Frederiksen, T. Identifying Highly Conducting Au-C Links through Inelastic Electron Tunneling Spectroscopy. *J. Phys. Chem. C* **2014**, *118*, 27106−27112.
(36) Foti, G.; Vázquez, H. Tip-Induced Gating of Molecular Levels in Carbene-Based Junctions. *Nanotechnology* **2016**, *27*, 125702.
(37) Gunst, T.; Lü, J.-T.; Hedegård, P.; Brandbyge, M. Phonon Excitation and Instabilities in Biased Graphene Nanoconstrictions. *Phys. Rev. B: Condens. Matter Mater. Phys.* **2013**, *88*, 161401.
(38) Datta, S. *Electronic Transport in Mesoscopic Systems*; Cambridge University Press: Cambridge, 1995.
(39) Frederiksen, T.; Paulsson, M.; Brandbyge, M.; Jauho, A.-P. Inelastic Transport Theory from First Principles: Methodology and Application to Nanoscale Devices. *Phys. Rev. B: Condens. Matter Mater. Phys.* **2007**, *75*, 205413.
(40) Foti, G.; Sánchez-Portal, D.; Arnau, A.; Frederiksen, T. Role of *k*-Point Sampling in the Supercell Approach to Inelastic Electron Tunneling Spectroscopy Simulations of Molecular Monolayers. *Phys. Rev. B: Condens. Matter Mater. Phys.* **2015**, *91*, 035434.
(41) Paulsson, M.; Frederiksen, T.; Brandbyge, M. Modeling Inelastic Phonon Scattering in Atomic- and Molecular-Wire Junctions. *Phys. Rev. B: Condens. Matter Mater. Phys.* **2005**, *72*, 201101.
(42) Härtle, R.; Thoss, M. Vibrational Instabilities in Resonant Electron Transport through Single-Molecule Junctions. *Phys. Rev. B: Condens. Matter Mater. Phys.* **2011**, *83*, 125419.
(43) Simine, L.; Segal, D. Vibrational Cooling, Heating, and Instability in Molecular Conducting Junctions: Full Counting Statistics Analysis. *Phys. Chem. Chem. Phys.* **2012**, *14*, 13820−13834.
(44) Xu, B.; Xiao, X.; Tao, N. J. Measurements of Single-Molecule Electromechanical Properties. *J. Am. Chem. Soc.* **2003**, *125*, 16164−16165.
(45) Arroyo, C. R.; Leary, E.; Castellanos-Gómez, A.; Rubio-Bollinger, G.; González, M. T.; Agraït, N. Influence of Binding Groups on Molecular Junction Formation. *J. Am. Chem. Soc.* **2011**, *133*, 14313−14319.
(46) Frei, M.; Aradhya, S. V.; Hybertsen, M. S.; Venkataraman, L. Linker Dependent Bond Rupture Force Measurements in Single-Molecule Junctions. *J. Am. Chem. Soc.* **2012**, *134*, 4003−4006.

DOI: 10.1021/acs.jpcc.6b11955
J. Phys. Chem. C 2017, 121, 1082−1088

(47) Yelin, T.; Vardimon, R.; Kuritz, N.; Korytár, R.; Bagrets, A.; Evers, F.; Kronik, L.; Tal, O. Atomically Wired Molecular Junctions: Connecting a Single Organic Molecule by Chains of Metal Atoms. *Nano Lett.* **2013**, *13*, 1956−1961.
(48) French, W. R.; Iacovella, C. R.; Rungger, I.; Souza, A. M.; Sanvito, S.; Cummings, P. T. Atomistic Simulations of Highly Conductive Molecular Transport Junctions Under Realistic Conditions. *Nanoscale* **2013**, *5*, 3654−3659.
(49) Balogh, Z.; Makk, P.; Halbritter, A. Alternative Types of Molecule-Decorated Atomic Chains in Au-CO-Au Single-Molecule Junctions. *Beilstein J. Nanotechnol.* **2015**, *6*, 1369−1376.
(50) Brandbyge, M.; Mozos, J.-L.; Ordejón, P.; Taylor, J.; Stokbro, K. Density-Functional Method for Nonequilibrium Electron Transport. *Phys. Rev. B: Condens. Matter Mater. Phys.* **2002**, *65*, 165401.
(51) Soler, J. M.; Artacho, E.; Gale, J. D.; García, A.; Junquera, J.; Ordejón, P.; Sánchez-Portal, D. The SIESTA Method for Ab Initio Order-N Materials Simulation. *J. Phys.: Condens. Matter* **2002**, *14*, 2745.
(52) Perdew, J. P.; Burke, K.; Ernzerhof, M. Generalized Gradient Approximation Made Simple. *Phys. Rev. Lett.* **1996**, *77*, 3865−3868.
(53) Paulsson, M.; Brandbyge, M. Transmission Eigenchannels from Nonequilibrium Green's Functions. *Phys. Rev. B: Condens. Matter Mater. Phys.* **2007**, *76*, 115117.
(54) Lorente, N.; Persson, M. Theory of Single Molecule Vibrational Spectroscopy and Microscopy. *Phys. Rev. Lett.* **2000**, *85*, 2997−3000.
(55) Troisi, A.; Ratner, M. A. Molecular Transport Junctions: Propensity Rules for Inelastic Electron Tunneling Spectra. *Nano Lett.* **2006**, *6*, 1784−1788.
(56) Gagliardi, A.; Solomon, G. C.; Pecchia, A.; Frauenheim, T.; Di Carlo, A.; Hush, N. S.; Reimers, J. R. A Priori Method for Propensity Rules for Inelastic Electron Tunneling Spectroscopy of Single-Molecule Conduction. *Phys. Rev. B: Condens. Matter Mater. Phys.* **2007**, *75*, 174306.
(57) Paulsson, M.; Frederiksen, T.; Ueba, H.; Lorente, N.; Brandbyge, M. Unified Description of Inelastic Propensity Rules for Electron Transport through Nanoscale Junctions. *Phys. Rev. Lett.* **2008**, *100*, 226604.
(58) Garcia-Lekue, A.; Sanchez-Portal, D.; Arnau, A.; Frederiksen, T. Simulation of Inelastic Electron Tunneling Spectroscopy of Single Molecules with Functionalized Tips. *Phys. Rev. B: Condens. Matter Mater. Phys.* **2011**, *83*, 155417.
(59) Foti, G.; Vázquez, H. Mapping the Intramolecular Contributions to the Inelastic Electron Tunneling Signal of a Molecular Junction. *Phys. Rev. B: Condens. Matter Mater. Phys.* **2016**, *94*, 045418.
(60) Bürkle, M.; Hellmuth, T. J.; Pauly, F.; Asai, Y. First-Principles Calculation of the Thermoelectric Figure of Merit for [2,2]-Paracyclophane-Based Single-Molecule Junctions. *Phys. Rev. B: Condens. Matter Mater. Phys.* **2015**, *91*, 165419.
(61) Gagliardi, A.; Romano, G.; Pecchia, A.; Di Carlo, A.; Frauenheim, T.; Niehaus, A. T. Electron-Phonon Scattering in Molecular Electronics: From Inelastic Electron Tunnelling Spectroscopy to Heating Effects. *New J. Phys.* **2008**, *10*, 065020.
(62) Segal, D.; Nitzan, A.; Hänggi, P. Thermal Conductance Through Molecular Wires. *J. Chem. Phys.* **2003**, *119*, 6840−6855.

DOI: 10.1021/acs.jpcc.6b11955
J. Phys. Chem. C 2017, 121, 1082−1088